

Interactions between fractional solitons in bimodal fiber cavities

Thawatchai Mayteearunyoo¹, and Boris A. Malomed^{2,3}

¹*Department of Electrical and Computer Engineering,*

Faculty of Engineering, Naresuan University, Phitsanulok 65000, Thailand

²*Department of Physical Electronics, School of Electrical Engineering, Faculty of Engineering, and the Center for Light-Matter University, Tel Aviv University, Tel Aviv, Israel*

³*Instituto de Alta Investigación, Universidad de Tarapacá, Casilla 7D, Arica, Chile*

We report results of systematic investigation of dynamics featured by moving two-dimensional (2D) solitons generated by the fractional nonlinear Schrödinger equation (FNLSE) with the cubic-quintic nonlinearity. The motion of solitons is a nontrivial problem, as the fractional diffraction breaks the Galilean invariance of the underlying equation. The addition of the defocusing quintic term to the focusing cubic one is necessary to stabilize the solitons against the collapse. The setting presented here can be implemented in nonlinear optical waveguides emulating the fractional diffraction. Systematic consideration identifies parameters of moving fundamental and vortex solitons (with vorticities 0 and 1 or 2, respectively) and maximum velocities up to which stable solitons persist, for characteristic values of the Lévy index which determines the fractionality of the underlying model. Outcomes of collisions between 2D solitons moving in opposite directions are identified too. These are merger of the solitons, quasi-elastic or destructive collisions, and breakup of the two colliding solitons into a quartet of secondary ones.

I. INTRODUCTION

In terms of abstract calculus, the concept of fractional derivatives was introduced by Niels Henrik Abel in 1823 [1], and by Joseph Liouville in 1832 [2]. In the modern mathematical literature [3], widely accepted is the Caputo's definition of the derivative of a non-integer positive order α [4],

$$\left(\frac{d}{dx}\right)^\alpha \psi = \frac{1}{\Gamma(1-\{\alpha\})} \int_0^x \frac{\psi^{(n)}(\xi) dx}{(x-\xi)^{\{\alpha\}}}, \quad (1)$$

where $\psi(x)$ is a generic real function, $\psi^{(n)}$ is the usual derivative of integer order $n \equiv [\alpha] + 1$, where $[\alpha]$ and $\{\alpha\} \equiv \alpha - [\alpha]$ are the integer and fractional parts of $[\alpha]$, and Γ is the Gamma-function.

In physics, fractional derivatives had appeared in the context of *fractional quantum mechanics* introduced by Laskin [5, 6]. The subject of that theory is the quantization, by means of the Feynman's path-integral technique [7], of the dynamics of particles whose classical stochastic motion is different from the usual Brownian form. Instead, the motion is performed by random *Lévy flights*, with the mean distance $|\bar{x}|$ of the particle from the initial position ($x = 0$) growing with time (in one dimension, 1D) as

$$|\bar{x}| \sim t^{1/\alpha}. \quad (2)$$

Here, parameter α , known as the *Lévy index* (LI), takes values

$$0 < \alpha \leq 2 \quad (3)$$

[8]. The usual Brownian random walk, with $|\bar{x}| \sim \sqrt{t}$, corresponds to the LI's limit value, $\alpha = 2$, while Eq. (2) with $\alpha < 2$ demonstrates that the $|\bar{x}|$ grows faster than \sqrt{t} at $t \rightarrow \infty$.

The Schrödinger equation for the wave function $\Psi(x, t)$ of the particle moving by Lévy flights in 1D, in the presence of a potential $V(x)$, was derived by Laskin [5, 6] in the following scaled form:

$$i \frac{\partial \Psi}{\partial t} = \frac{1}{2} \left(-\frac{\partial^2}{\partial x^2} \right)^{\alpha/2} \Psi + V(x) \Psi, \quad (4)$$

see also Ref. [9]. The fractional derivative, which represents the kinetic-energy term in Eq. (4), is different from the abstract Caputo's definition (1). Instead, it naturally arises as the *Riesz derivative* [10], which is built as the

superposition of the direct and inverse Fourier transforms ($x \rightarrow p \rightarrow x$),

$$\left(-\frac{\partial^2}{\partial x^2}\right)^{\alpha/2} \Psi = \frac{1}{2\pi} \int_{-\infty}^{+\infty} dp |p|^\alpha \int_{-\infty}^{+\infty} d\xi e^{ip(x-\xi)} \Psi(\xi). \quad (5)$$

In the framework of this definition, the action of the fractional kinetic-energy operator, $(-\partial^2/\partial x^2)^{\alpha/2}$, in the Fourier representation amounts to the straightforward multiplication by $|p|^\alpha$, with $|p|^\alpha$ being an obvious Fourier-space counterpart of this operator.

In the 2D space, the fractional Schrödinger equation for the wave function $\Psi(x, y)$ is a straightforward extension of Eq. (4) [6]:

$$i \frac{\partial \Psi}{\partial t} = \frac{1}{2} \left(-\frac{\partial^2}{\partial x^2} - \frac{\partial^2}{\partial y^2}\right)^{\alpha/2} \Psi + V(x, y) \Psi. \quad (6)$$

In the Fourier space with wavenumbers (p, q) , the action of the fractional operator, which represents the 2D kinetic energy, amounts to the multiplication by $(p^2 + q^2)^{\alpha/2}$, the explicit integral form of the operator in the coordinate space being

$$\left(-\frac{\partial^2}{\partial x^2} - \frac{\partial^2}{\partial y^2}\right)^{\alpha/2} \Psi = \frac{1}{(2\pi)^2} \int \int dp dq (p^2 + q^2)^{\alpha/2} \int \int d\xi d\eta e^{i[p(x-\xi) + iq(y-\eta)]} \Psi(\xi, \eta), \quad (7)$$

cf. Eq. (5).

Stationary solutions to Eq. (6), with real energy eigenvalue μ , are looked for in the usual form,

$$\Psi(x, y, t) = e^{-i\mu t} U(x, y), \quad (8)$$

where function U satisfies the stationary equation,

$$\mu U = \frac{1}{2} \left(-\frac{\partial^2}{\partial x^2} - \frac{\partial^2}{\partial y^2}\right)^{\alpha/2} U + V(x, y) U, \quad (9)$$

or the 1D reduction of Eq. (9). Function U is real for the ground-state solution, and complex for excited states carrying the vorticity (angular momentum).

It is relevant to mention that, in the framework of the mean-field theory, the dynamics of Bose-Einstein condensates in ultracold atomic gases is governed by the Gross-Pitaevskii equation (GPE), i.e., the Schrödinger equation for the single-particle wave function augmented by the cubic term $\sim |\Psi|^2 \Psi$ which represents the mean-field effect of inter-particle collisions [11]. A challenging possibility is to consider a condensate of bosonic particles obeying the fractional Schrödinger equation (6) or its one-dimensional reduction (4). While a consistent derivation of the respective fractional GPE remains an open problem, it is expected that the equation may be obtained the following scaled form:

$$i \frac{\partial \Psi}{\partial t} = \frac{1}{2} \left(-\frac{\partial^2}{\partial x^2} - \frac{\partial^2}{\partial y^2}\right)^{\alpha/2} \Psi + V(x, y) \Psi + \sigma |\Psi|^2 \Psi, \quad (10)$$

with $\sigma = +1$ or -1 corresponding to the repulsive or attractive sign of the inter-particle interactions, respectively [21].

II. THE BASIC MODEL

Thus far, fractional quantum mechanics has not been observed experimentally. An alternative possibility of the physical realization of the fractional Schrödinger equation was proposed by Longhi [12], following the commonly known similarity of the Schrödinger equation in quantum mechanics and the paraxial propagation equation for the classical optical field, with time t replaced by the propagation distance, z [13]. The setup proposed for the realization of this possibility is based on the $4f$ (four-focal-lengths) structure implemented in an optical cavity [12]. The central element is a phase mask, placed in the middle (Fourier) plane of the cavity. A lens decomposes the beam's transverse structure into its Fourier components with wavenumbers (p, q) . Then, the distance from the optical axis of the point at which each component passes the phase mask is, roughly speaking, $R \sim \sqrt{p^2 + q^2}$. The action of the effective fractional diffraction on the Fourier transform $\hat{\Psi}(p, q)$ of the optical beam amounts, according to Eq. (5) or (7), to

the local phase shift

$$\hat{\Psi}(p, q) \rightarrow \hat{\Psi}(p, q) \exp \left[i (p^2 + q^2)^\alpha Z \right], \quad (11)$$

where Z is the propagation distance over which the effect of the fractional diffraction is accumulated. In the proposed setup, the corresponding differential phase shift is provided by the design of the phase mask. In addition to that, the effect corresponding to potential $V(x, y)$ in Eq. (6) (or in its one-dimensional counterpart (4)) can be emulated by a specially shaped mirror added to the cavity setup [12].

The setting which is outlined above provides a single-stage transformation of the optical beam, which is represented, essentially, by Eq. (11). The continuous fractional Schrödinger equation (6) or (4) is then introduced as a result of averaging over many cycles of the intra-cavity circulation of light.

Experimental implementation of the setup realizing the effectively fractional diffraction has not yet been reported. However, a recent experimental work has implemented the realization of a similarly devised scheme which demonstrates the effective fractional group-velocity dispersion in a fiber-laser cavity, in which the differential phase shift of decomposed temporal spectral components, emulating the action of the fractional dispersion, was provided by a computer-generated hologram, inserted as the central phase mask [14].

Once the effective fractional diffraction can be implemented by means of the light propagation in the (1+1)- and (2+1)-dimensional spatial domains, with the transverse dimensions 1 and 2, respectively (here, +1 stands for the propagation direction z), it is natural to include nonlinearity of the optical medium, and thus introduce the fractional nonlinear Schrödinger equation (FNLSE) [15, 16]. In the case of the cubic (Kerr) nonlinearity [13], its scaled form is tantamount to the conjectured fractional GPE (10). Further, the presence of the self-focusing nonlinearity suggests a possibility to predict the existence of fractional solitons, as stable solutions of the FNLSEs [17–21]. A crucially important problem for the stability of such solitons is the possibility of the onset the *wave collapse* in the FNLSE. Indeed, an elementary estimate demonstrates that the one-dimensional FNLSE with LI α and the cubic self-focusing term gives rise to the *critical collapse* (which is initiated by an input whose norm exceeds a final critical value [22, 23]) in the case of $\alpha = 1$, and to the *supercritical collapse* (which may be initiated by the input with an arbitrarily small norm) in the case of $\alpha < 1$. Thus, the one-dimensional cubic FNLSE may give rise to stable solitons in the interval of $1 < \alpha \leq 2$, including the usual (non-fractional) NLSE with $\alpha = 2$.

The two-dimensional FNLSE with the cubic self-focusing term is problematic, as it leads to the critical collapse in the usual case of $\alpha = 2$ (with the commonly known stationary solutions in the form of unstable *Townes solitons* [22–24]), and to the supercritical collapse, hence strongly unstable solitons, in the case of $\alpha < 2$. A solution of the instability problem for the 2D solitons is the use of the cubic-quintic (CQ) nonlinearity. In that case, the trend towards the collapse, driven by the cubic self-focusing, is arrested by the higher-order quintic defocusing term. This option is a relevant one, as the combination of cubic and quintic terms provides an accurate approximation for the nonlinearity of various optical media, such as chalcogenide glasses [25], liquid carbon disulfide [26], colloidal suspensions of metallic nanoparticles [27], and epsilon-near-zero waveguides [28]. The respective (2+1)-dimensional FNLSE for the paraxial evolution of amplitude $u(x, y; z)$ of the electromagnetic wave is

$$i \frac{\partial u}{\partial z} = \frac{1}{2} \left(-\frac{\partial^2}{\partial x^2} - \frac{\partial^2}{\partial y^2} \right)^{\alpha/2} u - |u|^2 u + |u|^4 u, \quad (12)$$

where the fractional-diffraction operator is defined as per Eq. (7), and coefficients in front of the self-focusing cubic and defocusing quintic terms are set equal to 1 by means of rescaling.

Stationary soliton solutions to Eq. (12) with real propagation constant $k > 0$ are looked for as

$$u(x, y; z) = e^{ikz} \phi(x, y), \quad (13)$$

where $\phi(x, y)$ is a localized solution of equation

$$k\phi + \frac{1}{2} \left(-\frac{\partial^2}{\partial x^2} - \frac{\partial^2}{\partial y^2} \right)^{\alpha/2} \phi - |\phi|^2 \phi + |\phi|^4 \phi = 0. \quad (14)$$

Soliton solutions are characterized by the integral power,

$$P = \int \int |u(x, y, \tau)|^2 dx dy. \quad (15)$$

In the case of the non-fractional diffraction, $\alpha = 2$, Eq. (14) gives rise to families of 2D solitons with embedded

integer vorticity (winding number), $m \geq 0$ ($m = 0$ corresponds to the fundamental solitons). In polar coordinates (r, θ) , the vortex-soliton solutions are looked for as $\phi(r, \theta) = a(r) \exp(im\theta)$, where the real amplitude $a(r)$ satisfies the radial equation $(a'' + r^{-1}a' - m^2r^{-2}a) - 2(ka - a^3 + a^5) = 0$, supplemented by the boundary conditions $a(r) \sim r^m$ at $r \rightarrow 0$, and $a(r) \sim r^{-1/2} \exp(-\sqrt{-2k}r)$ at $r \rightarrow \infty$. For all winding numbers $m = 0, \pm 1, \pm 2, \dots$, 2D vortex solitons exist in the interval of values of the propagation constant

$$0 < k < 3/16, \quad (16)$$

in which the power takes values $0 < P < \infty$. In the limit of $k \rightarrow 3/16$, the soliton develops an indefinitely broad flat-top shape, with the inner amplitude approaching the limit value

$$(|\phi|)_{\max}(k = 3/16) = \sqrt{3}/2. \quad (17)$$

The entire family of the fundamental solitons, with $m = 0$, is completely stable, while each family of the vortex solitons has its specific stability interval, $k_{\min}^{(m)} < k < 3/16$, where the power is large enough [29]. The stability interval shrinks with the increase of m , viz., $k_{\min}^{(1)} \approx 0.1487$, $k_{\min}^{(2)} \approx 0.1618$, $k_{\min}^{(3)} \approx 0.1700$ [30].

Solutions of 1D FNLSEs with the CQ nonlinearity and, in some cases, with potential terms, were studied in detail, including solitons [31]-[37], breathers [38], Airy waves [39], and modulational instability [40]. In 2D, systematic results have been reported for solitons, including “unconventional” ones [41, 42], solitary vortices [43] and necklace clusters [44]. As well as the non-fractional CQ NLSE (with $\alpha = 2$), its 2D fractional counterpart, with $\alpha < 2$, produces fundamental and vortex solitons in interval (16); however, the difference is that, in the case of $\alpha < 2$, the solitons exist with the power exceeding a certain minimum value [43] (for illustration, see Figs. 1(a), 4(a), and 6(a) below). Accordingly, curves $P(k)$ feature two segments, one with $dP/dk > 0$, which satisfies the celebrated Vakhitov-Kokolov (VK) criterion [22, 23, 45], and another one, with $dP/dk < 0$. The latter segment is definitely unstable, as it does not comply with the VK criterion. The branch of the fundamental-soliton family ($m = 0$) with $dP/dk > 0$ is completely stable, while this condition is only necessary but not sufficient for the stability of the vortex-soliton families with $|m| \geq 1$, only their parts with the power large enough, $P > P_{\min}^{(m)}(\alpha)$, being stable [43]. The stability-threshold value, $P_{\min}^{(m)}(\alpha)$, grows with the increase of the FNLSE’s fractionality, i.e., with the decrease of LI α , thus making the creation of stable vortex solitons more difficult for smaller α .

The first subject of the present work, addressed below in Section 3, is the creation of moving 2D solitons (actually, these are tilted spatial solitons) as solutions of Eq. (12) with winding numbers $m = 0, 1$, and 2 and coordinate x replaced by x by $x' = x - cz$, where real c is the “velocity” (actually, the spatial tilt). It is enough to consider the tilt only along coordinate x , as the tilt in any other direction is equivalent to it in the isotropic system. Accordingly, Eq. (12) is rewritten in the moving (tilted) coordinates:

$$i \frac{\partial u}{\partial z} - ic \frac{\partial u}{\partial x} = \frac{1}{2} \left(-\frac{\partial^2}{\partial x^2} - \frac{\partial^2}{\partial y^2} \right)^{\alpha/2} u - |u|^2 u + |u|^4 u. \quad (18)$$

Stationary solutions to Eq. (18) are looked for in the usual form, i.e., as per Eq. (13), where function $\phi(x, y)$ satisfies the equation

$$k\phi + ic \frac{\partial \phi}{\partial x} + \frac{1}{2} \left(-\frac{\partial^2}{\partial x^2} - \frac{\partial^2}{\partial y^2} \right)^{\alpha/2} \phi - |\phi|^2 \phi + |\phi|^4 \phi = 0, \quad (19)$$

Note that, unlike the quiescent (untitled) solitons with $c = 0$, solutions of Eq. (19) with $c > 0$ cannot be real.

The essential difference of the FNLSE from its non-fractional counterpart, with $\alpha = 2$, is that the fractional diffraction operator (7) (as well as its 1D counterpart (5)) breaks the Galilean invariance, hence Eqs. (18) and (19) cannot be transformed back into the original ones (12) and (14), respectively. A result reported below is that stable moving solitons exist up to a certain maximum velocity, c_{\max} , which depends on LI α and propagation constant k , as well as on winding number m . At $c > c_{\max}$, the fundamental 2D solitons do not exist, while the vortex ones, with $m = 1$ and 2, may exist, but are unstable.

Once stable moving solitons are available, the next relevant problem, which is addressed below in Section 4, is collisions between the solitons moving (tilted) in opposite directions. It is demonstrated that outcomes of the collisions between fundamental solitons may be quasi-elastic or strongly inelastic, leading to merger of the solitons, or their decay, or, depending on the parameters, breakup of the two colliding solitons into a set of four ones. The latter outcome is also found, as a generic one, for collisions between counterpropagating vortex solitons, with identical or opposite winding numbers, alike, i.e., $m_1 = m_2 = 1$, or $m_{1,2} = \pm 1$.

III. MOVING SOLITONS AND VORTICES

A. Fundamental solitons ($m = 0$)

Numerical solutions of Eq. (19) for stationary solitons have been obtained by means of the modified squared-operator method [46]. The computational domain in the (x, y) plane was taken as a square of size $|x|, |y| < 200$, discretized by sets of 2^9 points along each dimension. Then, stability of the so produced solutions was verified by means of direct simulations of Eq. (18).

1. The moving fundamental solitons for the Lévy index (LI) $\alpha = 1.5$

For the traveling (tilted) fundamental 2D solitons (with $m = 0$), the results are presented here for two characteristic LI values, $\alpha = 1.0$ and 1.5 , which produce solutions of the FNLSE which are sufficiently different from the well-known family of solutions obtained from Eq. (12) with the ordinary nonfractional diffraction, i.e., $\alpha = 2$.

For $\alpha = 1.5$, the summary of the numerically generated results is presented in Fig. 1. The main plot in panel (a) reproduces, for the reference's sake, the plot $P(k)$ for the family of the fundamental quiescent (untitled, $c = 0$) solitons, which is the same as reported (in a different notation) in Ref. [44]. As mentioned above, the subfamilies with $dP/dk > 0$ and $dP/dk < 0$ are, respectively, stable and unstable, in full compliance with the VK criterion. The first set of new results for the moving (tilted) 2D fundamental solitons is reported by means of the inset in Fig. 1(a), *viz.*, the largest value c_{\max} of velocity c in Eq. (19) up to which the numerical solution of this equation produces solitons. Detailed results for families of the moving stable fundamental solitons are summarized in Figs. 1(b,c,d) by means of dependences of the power P , amplitude ϕ_{\max} , and widths W_{FWHM} in the direction of motion, x , and in the perpendicular direction, y , on velocity, c , for several fixed values of the propagation constant, k . In these figures, the curves terminate at points $c = c_{\max}$ (in compliance with the inset in Fig. 1(a)), beyond which numerical solutions for the moving solitons could not be found. In addition, Fig. 1(b) shows the smallest value of the power, P_{\min} , up to which moving solitons are found for given c (actually, considered as c_{\max}) and any value of k .

Typical examples of stable moving solitons with $\alpha = 1.5$ are displayed in Fig. 2. Both Figs. 1 and 2 demonstrate that the increase of the velocity (tilt) leads to monotonous decrease of their amplitude and power. As concerns the width of the fundamental solitons, Fig. 1(d) demonstrates its nonmonotonous behavior, *viz.*, originally the solitons shrink with the increase of the velocity, changing to expansion after reaching a minimum value of the width. In this connection, it is relevant to note that the increase of the solitons' width at $c \rightarrow c_{\max}$ makes it difficult to find them in a numerically exact form. At small c , Fig. 2 manifests the above-mentioned trend to the formation of the fundamental solitons with the flat-top profile.

As concerns unstable solitons, which, in the case of $c = 0$, populate the segment of the $P(k)$ curve in Fig. 1(a) with $dP/dk < 0$, a typical outcome of the development of the instability is spontaneous transformation of the stationary fundamental soliton into a robust breather, as shown in Fig. 3. At $k < 0.01$, the unstable fundamental soliton does not evolve into a breather, but decays (not shown here in detail).

2. The moving fundamental solitons for the Lévy index (LI) $\alpha = 1.0$

For an essentially smaller value of the LI, $\alpha = 1.0$, the results for families of quiescent and moving 2D fundamental solitons are collected in Fig. 4, following the pattern of Fig. 1 for $\alpha = 1.5$. Here too, the curves plotted in panels (b)-(d) terminate at points $c = c_{\max}$ (in compliance with the inset to panel (a)), beyond which solutions for the moving soliton could not be found. Further, it is seen that the dependence of c_{\max} on k in the inset to Fig. 4(a), and the dependence of the power on the velocity (tilt) c , are similar to those shown in Fig. 1 for $\alpha = 1.5$. However, the dependences of the amplitude and width on c , observed in Figs. 4(c) and (d), are drastically different from the case of $\alpha = 1$: the amplitude does not decrease, but slowly increases with c , while the width decreases monotonously, without the switch to increase (cf. Fig. 1(d) for $\alpha = 1.5$).

Typical examples of stable moving (tilted) solitons, with different values of velocity (tilt) c , for $\alpha = 1.0$ and fixed propagation constant $k = 0.09$, are displayed in Fig. 5. In comparison with the case of $\alpha = 1.5$, the above-mentioned difference is that the soliton's amplitude almost does not depend on c , while the shape keeps shrinking with the increase of c . In this case, unstable solitons also tend to spontaneously transform into oscillatory modes, cf. Fig. 3 (not shown here in detail).

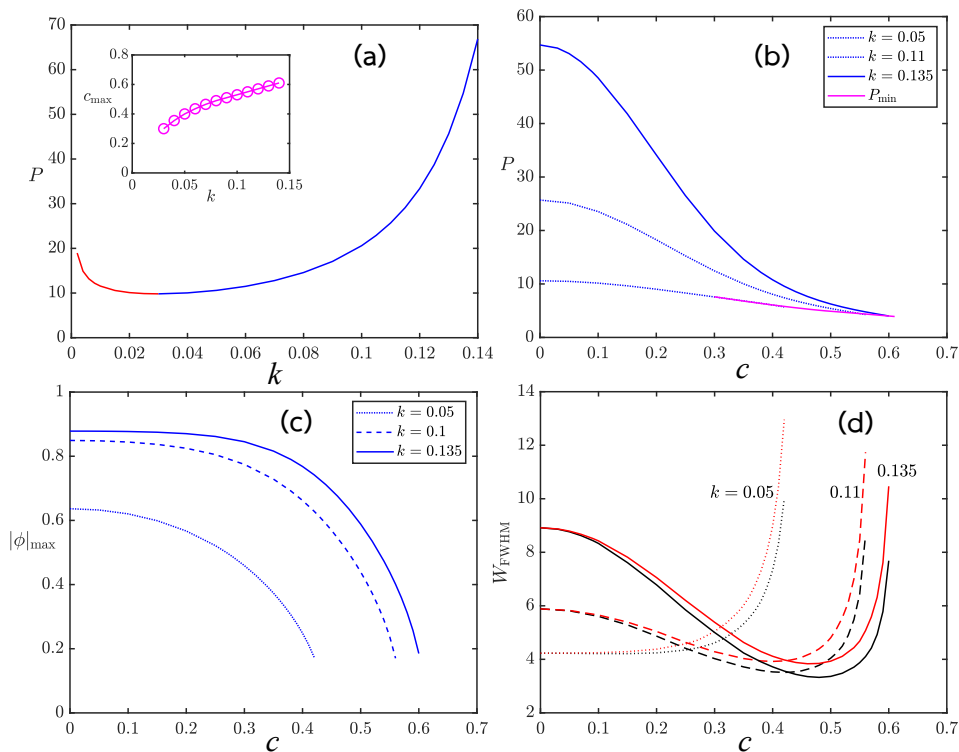


FIG. 1. Numerical results for the stable 2D fundamental solitons (with zero vorticity) produced by Eq. (19) with LI $\alpha = 1.5$. (a) Power P of the quiescent (untilted) solitons (corresponding to $c = 0$ in Eq. (19)) vs. their propagation constant, k . The inset shows the largest velocity (tilt) c_{\max} , up to which the moving solitons exist for given k . Other panels show the power P (b), amplitude $|\phi|_{\max}$ (c), and full width at half-maximum W_{FWHM} in the x and y directions (shown by the black and red curves, respectively) (d), vs. the velocity (tilt) c , for different fixed values of k . In panel (b), P_{\min} (c) is the smallest value of the power for which the moving solitons are found for given c , considered as c_{\max} , with any value of k .

B. Vortices ($m = 1$ and 2)

For vortex solitons, systematic results have been collected for $m = 1$ and $\alpha = 1.5$. Stable vortex modes exist also for $m \geq 2$ at $\alpha = 1.5$, and for $m = 1$ at $\alpha = 1.0$, but they are stable at very large values of the power [43]. Because the inner amplitude of the modes cannot exceed the maximum value (17), this implies the necessity to construct solutions in very large spatial domains, which makes the numerical computations challenging.

Following the pattern of Figs. 1 and 4, characteristics of the family of the vortex solitons with $m = 1$ and fixed propagation constant, $k = 0.14$, are presented in Fig. 6. Stable and unstable vortex solitons populate the blue and red segments of the $P(k)$ curve in panel (a). Unlike the families of the fundamental solitons (cf. Figs. 1(a) and 4(b)), Fig. 6(a) demonstrates that the VK criterion is not sufficient for the stability of the vortex solitons, because their instability against spontaneous splitting (see Fig. 8 below) is accounted for by complex eigenvalues, which are not taken into regard by the VK condition [30, 43].

Overall, the dependences $P(c)$ and $|\phi|_{\max}(c)$ for the vortex solitons, plotted in Figs. 6(b) and (c), are qualitatively similar to the same dependences for the fundamental solitons in Figs. 1(b) and (c), while the dependence of the widths on c in Fig. 6(d) is a monotonously decreasing one, in contrast with its nonmonotonous counterpart for the fundamental solitons at the same value of the LI, $\alpha = 1.5$. Also different are the dependences $c_{\max}(k)$ for the fundamental and vortex solitons: as one sees from the comparison of insets in Figs. 1(a) and 6(a), this dependence is strong in the former case, and very weak in the latter one.

The meaning of the value $P_{\min}(c)$ for the moving vortex solitons, which is shown in panel (b), is different from that of $P_{\min}(c)$ for the fundamental solitons (cf. Figs. 1(b) and 4(b)): while the fundamental solitons do not exist at $P < P_{\min}$, their vortex counterparts may exist at $P < P_{\min}$, but they are unstable against spontaneous splitting, as shown below in Fig. 9.

A peculiarity of the dependence of the amplitude on c for the vortex soliton, observed in Fig. 6(c), is that it is non-smooth, showing, in particular, a conspicuous irregularity around $c = 0.172$. However, this feature is not a significant one, as it belongs to the unstable segment of the family, according to Fig. 6(b).

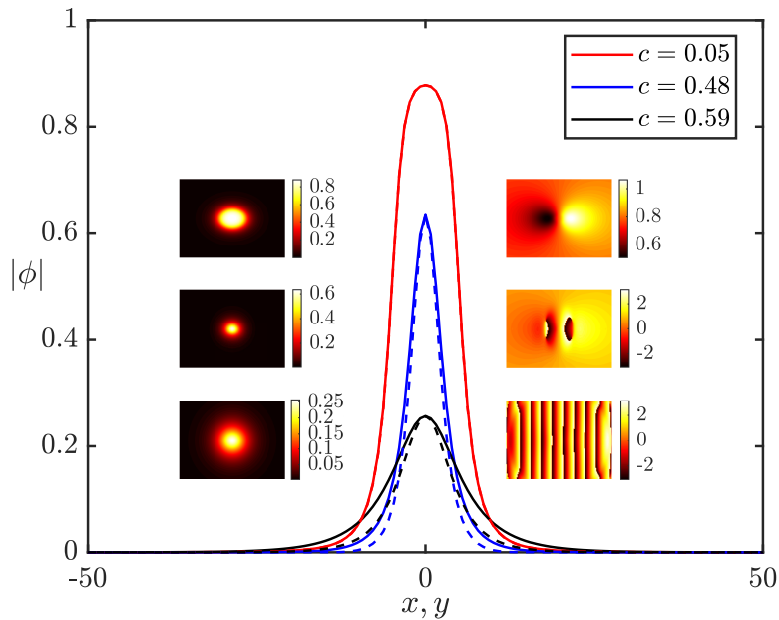


FIG. 2. Amplitude profiles of the stable moving (tilted) fundamental solitons with fixed LI $\alpha = 1.5$ and propagation constant $k = 0.135$, for different profiles of the velocity (tilt) c . The dashed and solid lines represent the profiles along the x - and y -axes, respectively. Insets display top views of the 2D amplitude and phase shapes (the left and right plots, respectively). The top, middle, and bottom inset rows correspond, severally, to $c = 0.05, 0.48$, and 0.59 .

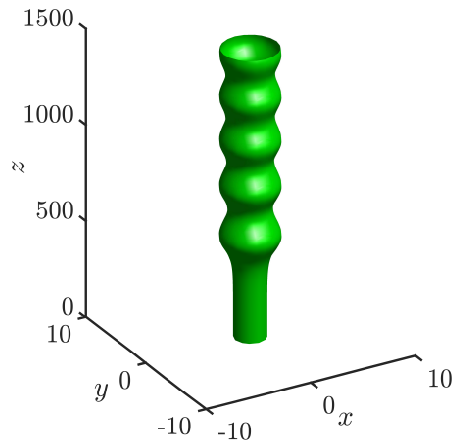


FIG. 3. The evolution of an unstable fundamental ($m = 0$) soliton with $c = 0$, $\alpha = 1.5$, and $k = 0.02$, produced by simulations of Eq. (12) and displayed by means of the isosurface of the local intensity, $|u(x, y)|^2 = 0.171$. The soliton spontaneously transforms into a breather.

Typical examples of stable and unstable quiescent ($c = 0$) and moving ($c > 0$) vortex solitons are displayed in Fig. 7. In addition, an example of the splitting instability of a quiescent vortex soliton with $k = 0.1$, which indeed belongs to the unstable subfamily in Fig. 6(a)), is displayed in Fig. 8. It breaks up into a set of two separating fragments, each one being close to a fundamental soliton. The picture demonstrates conversion of the spin momentum of the original vortex into the orbital angular momentum of the moving fragments. In addition to that, each secondary soliton exhibits weak elliptical deformation and inner spinning, which also carries a small fraction of the total momentum.

Moving vortices with $P < P_{\min}$ are unstable too, breaking up in two quasi-soliton fragments, which separate in the y direction (perpendicular to the velocity), as shown for $k = 0.14$ and $c = 0.2$ in Fig 9. The stationary profile of this unstable vortex soliton is displayed in Fig. 7.

For the sake of the completeness of the presentation, an example of the instability of the quiescent double-vortex soliton (with $m = 2$) is displayed in Fig. 10. As is typical for the instability of vortex solitons with the double winding number [30], the outcome is its fission into the set of four separating fragments, each one being a spinning elliptically

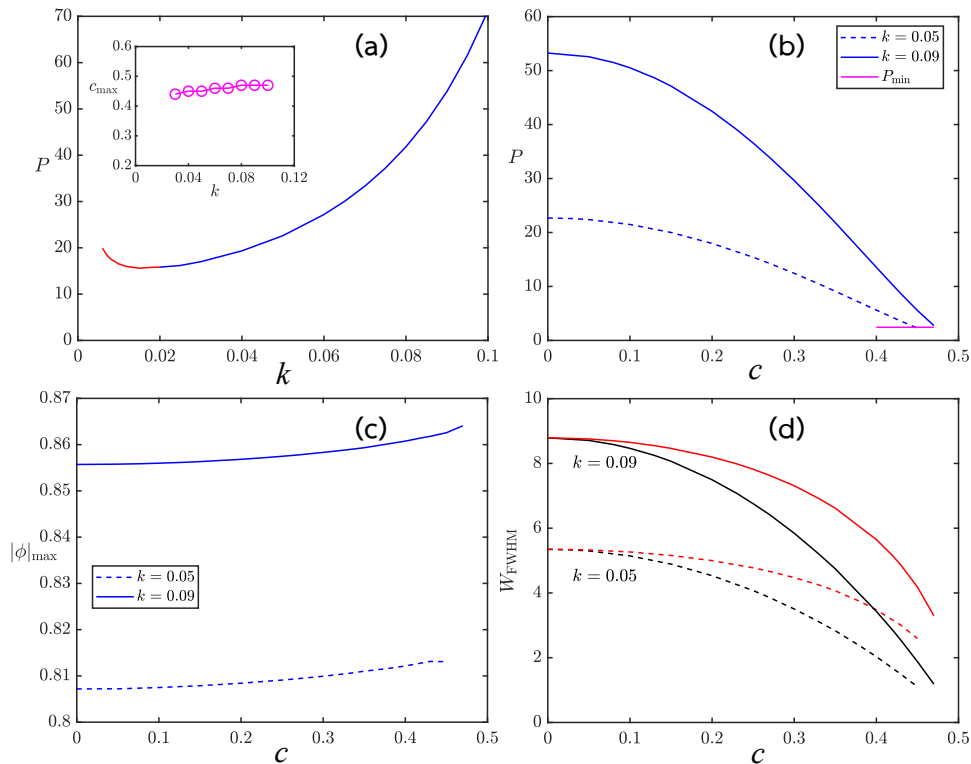


FIG. 4. The same as in Fig. 1, but for the family of the 2D fundamental solitons found for LI $\alpha = 1.0$. The fixed values of k are indicated in panels (b) - (d).

deformed fundamental soliton (cf. the spontaneous fission of the unstable vortex with $m = 1$ into the set of two quasi-soliton fragments, exhibited in Fig. 7).

In all the simulations performed in this work, moving double-vortex solitons, with $m = 2$, demonstrate splitting instability. However, it is different from the spontaneous fission of the quiescent vortex with $m = 2$ into the set of four quasi-solitons with equal powers (cf. Fig. 9): as shown in Fig. 11, three low-power jets split off from the central beam, which keeps a major share of the initial power, in the form of a deformed quasi-solitons featuring inner spinning.

IV. COLLISIONS BETWEEN MOVING SOLITONS

The availability of stably moving fundamental and vortex solitons suggests a possibility to study collisions between identical ones moving in opposite directions, $\pm x$. To this end, Eq. (12) was simulated, with the input in the form of a pair of identical solitons produced by numerical solutions of Eq. (19) with equal vorticities $m = 0$ or 1 and opposite velocities $\pm c$. Centers of the two solitons are initially placed at points $x = \pm x_0$, with a sufficiently large separation $2x_0$.

A. Collisions between fundamental solitons

First, setting $\alpha = 1.5$ in Eq. (12), we present results of the interaction between moving fundamental solitons with a fixed propagation constant, $k = 1.35$, and gradually increasing collision velocity $|c|$. For small values of the velocity, Figs. 1(b,d) and 2 demonstrate that the moving solitons have higher powers and relatively large widths. In this case, the simulations displayed in Fig. 12 reveal that the strong nonlinearity, caused by the large powers, leads to strongly inelastic outcomes of the collisions: the solitons colliding with velocities $c = \pm 0.1$ and ± 0.2 (Figs. 12(a,b)) merge into quiescent (standing) breathers, with the amplitude of inner oscillations decreasing with the increase of $|c|$. As an extension of this trend, Fig. 12(c) demonstrates that the collision with velocities $c = \pm 0.3$ leads to the merger of the colliding solitons into a single quiescent quasi-soliton, without conspicuous oscillations.

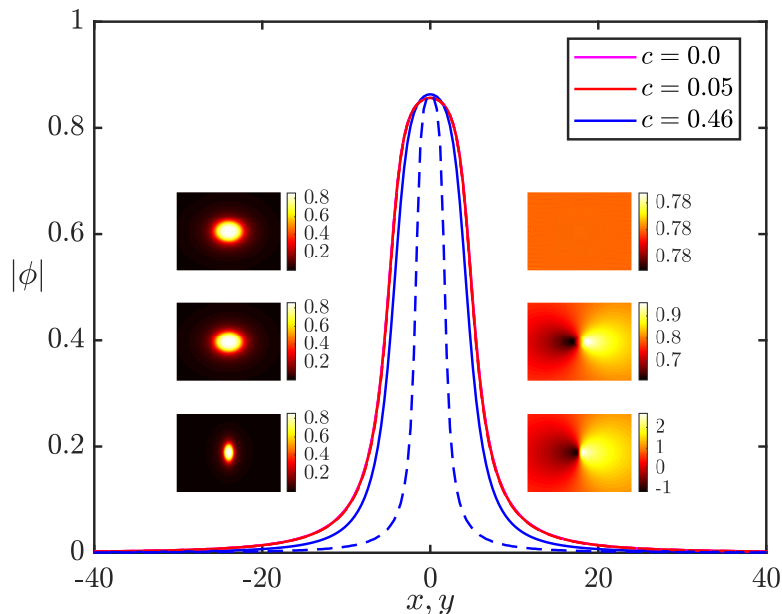


FIG. 5. The same as in Fig. 2, but for LI $\alpha = 1.0$ and fixed propagation constant $k = 0.09$.

Next, in the interval of the collision velocities

$$0.38 \leq |c| \leq 0.45 \quad (20)$$

the weaker nonlinearity, corresponding to the smaller power and amplitude (see Figs. 1(b) and (c)), is not sufficient to maintain the soliton into which the colliding ones attempt to merge, therefore it quickly decays, as shown in Fig. 12(d) for the collision with $c = \pm 0.40$. Thus, the collisions are completely destructive in interval (20). Note that the right edge of this interval is close to $c \approx 0.48$, at which the soliton's width attains a minimum, $(W_{\text{FWHM}})_{\text{min}}(\alpha = 1.5, k = 1.35) \approx 3.325$, in Fig. 1(d).

For the values of LI $\alpha = 1.50$ and propagation constant $k = 1.35$ which are considered here, the inset in Fig. 1(a) demonstrates that the moving fundamental solitons exist up to $c_{\text{max}}(\alpha = 1.5, k = 1.35) \approx 0.6$. In the interval of the collision velocities between the right edge of region (20) and c_{max} , the relatively large velocity and weak nonlinearity make the collisions quasi-elastic, as shown in Figs. 13(a) and (b) for $|c| = 0.50$ and 0.59 , respectively, the latter value being very close to c_{max} .

In simulations of collisions between fundamental solitons with smaller propagation constants (e.g., $k = 0.05$), hence much lower powers and amplitudes (see Figs. 1(b) and (c)), the merger does not occur. In most cases, the collisions are destructive, becoming quasi-elastic at $|c|$ close to the respective value c_{max} (not shown here in detail).

In the case of LI $\alpha = 1.0$, we take $k = 0.09$ as the value of the propagation constant corresponding to high power of the fundamental soliton, as suggested by Fig. 4(a). In this case, the simulations demonstrate merger of the colliding fundamental solitons into a breather at relatively small velocities. In the velocity interval

$$0.21 \leq |c| \leq 0.36, \quad (21)$$

the simulations reveal quasi-elastic collisions in a specific form: as shown in Fig. 14 for velocities $c = \pm 0.3$, the soliton colliding in the x -direction separate, after the collision, along the y axis, i.e., the velocity vectors rotate by 90° in the (x, y) plane.

At $\alpha = 1.0$, $k = 0.09$, and $|c| > 0.36$, up to $|c| = c_{\text{max}} \approx 0.49$ (see Fig. 4(b)), collisions between fundamental solitons are inelastic. The result, displayed in Fig. 15 for $c = 0.4$, demonstrates breakup of the colliding pair into a set of four secondary solitons, which move in oblique directions in the (x, y) plane.

B. Collisions between vortices ($m_1 = m_2 = 1$ and $m_1 = -m_2 = 1$)

Similar to what is shown in Fig. 15, collisions between identical counterpropagating vortex solitons with $\alpha = 1.5$ and winding numbers $m = 1$ lead, in the generic case, to their breakup into a set of four secondary quasi-solitons. An

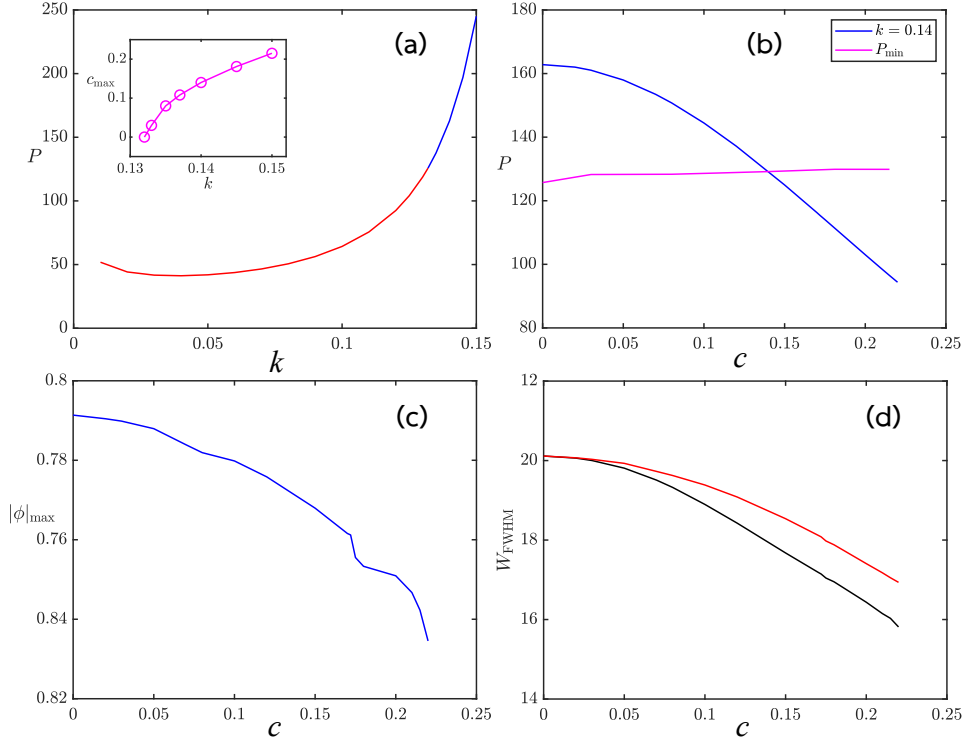


FIG. 6. (a) Power P of the quiescent (untitled) vortex solitons (corresponding to $c = 0$ in Eq. (19)) with $m = 1$ vs. the propagation constant k . The inset shows the largest velocity (tilt) c_{\max} , up to which stable moving vortex solitons exist for given k . Other panels show the power P (b), amplitude $|\phi|_{\max}$ (c), and full width at half-maximum W_{FWHM} in the x and y directions (shown by the black and red curves, respectively), vs. the velocity (tilt) c of the vortex solitons, for a fixed propagation constant, $k = 0.14$. In panel (b), P_{\min} (c) is the smallest value of the power for which the moving vortex solitons are stable for given c (considered as c_{\max}), with any value of k .

example for the colliding solitary vortices with propagation constant $k = 0.14$ (these vortices are stable, according to Fig. 6(a)), is displayed in Fig. 16 for velocities $c = \pm 0.1$. The emerging quartet of quasi-solitons feature non-circular shapes, each spinning counter-clockwise in the course of the propagation, to keep the angular momentum of the original vortices.

It is natural too to explore collisions between counter-rotating vortex solitons, with winding numbers $m = \pm 1$. The result is shown in Fig. 17, for the same values of the parameters, $k = 0.14$, $c = \pm 0.1$, and $\alpha = 1.5$, as in Fig. 16. The outcome is again fission of the colliding vortices into a set of four separating quasi-solitons. Nevertheless, an essential difference is that the lack of the necessity to keep the initial total angular momentum, which is zero in this case, allows all the emerging quasi-solitons to move in the direction of the original collision (along the x axis), while in Fig. 16 two of them are moving, essentially, in the perpendicular direction.

V. CONCLUSION

The objective of this work is to develop systematic analysis of dynamics initiated by motion of localized modes produced by the two-dimensional FNLSE (fractional nonlinear Schrödinger equation) with the CQ (cubic-quintic) nonlinearity. The motion problem is nontrivial for the FNLSE because the fractional diffraction does not admit Galilean invariance of the equation. The choice of the nonlinearity with competing self-focusing cubic and defocusing quintic terms is necessary to stabilize the localized modes, in the form of fundamental (zero-vorticity) and vortex solitons, against the collapse (however, the stability of the vortex solitons against spontaneous splitting into sets of fundamental quasi-solitons remains a nontrivial issue). The model can be implemented in optical cavities which combine the emulation of the fractional diffraction and CQ material nonlinearity.

By means of the systematic numerical analysis, parameters of stably moving fundamental and vortex solitons (with winding numbers $m = 0$ and 1 , respectively) and largest velocities, up to which the stable solitons exist, are identified, for characteristic values of the LI (Lévy index) which defines the fractionality of the underlying FNLSE.

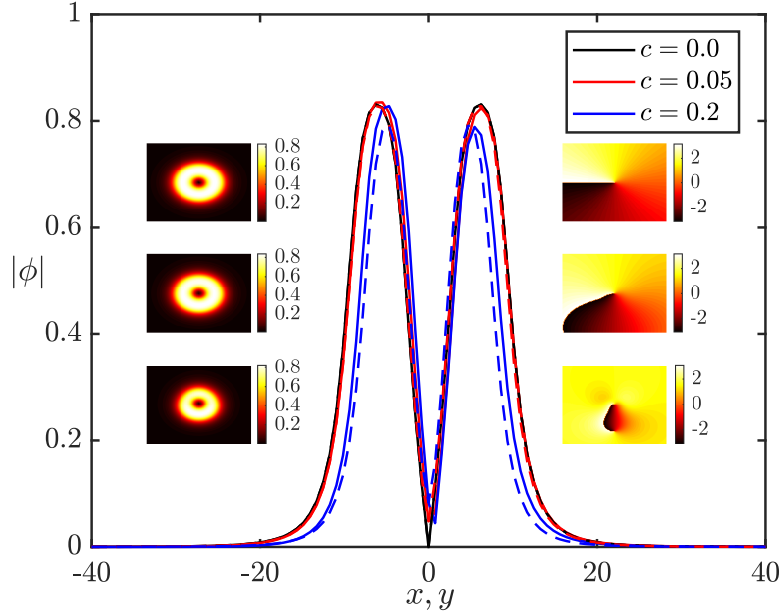


FIG. 7. Amplitude profiles of moving vortex solitons for the fixed propagation constant, $k = 0.14$, and different velocities. Dashed and solid lines represent the profiles in the x and y directions, respectively. The left and right inset panels are 2D plots of the amplitude and phase shapes. Top and middle rows represent stable vortex solitons with $c = 0$ and $c = 0.05$, respectively. The bottom row, with $c = 0.2$, corresponds to an unstable vortex soliton, in agreement with Fig. 6(b) (the power of this solutions is $P = 103.01 < P_{\min} \approx 129.17$). The unstable soliton spontaneously breaks up in two separating fragments, which are close to fundamental solitons, see Fig. 9.

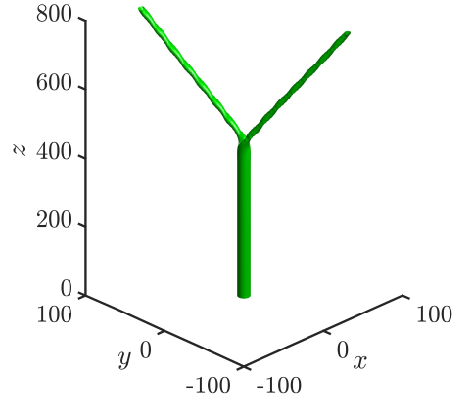


FIG. 8. The evolution of an unstable vortex soliton with $\alpha = 1.5$, $c = 0$ and $k = 0.1$, as produced by simulations of Eq. (12), is shown by means of the isosurface of the local intensity, $|u(x, y)|^2 = 0.357$. The vortex spontaneously splits in two obliquely moving modes which are close to stable fundamental solitons.

Then, collisions between counterpropagating 2D solitons are explored by means of numerical simulations. The results demonstrate different outcomes of the collisions, depending on parameters, *viz.*, merger of colliding solitons, quasi-elastic and destructive collisions, and the breakup of the colliding pairs into sets of four quasi-solitons. In the latter case, the colliding vortex solitons split into a quartet of spinning quasi-solitons.

The analysis reported in this work can be naturally extended in other directions. One of them is the consideration of the fractional 2D complex Ginzburg-Landau equation with the cubic-quintic nonlinearity, which may produce a variety of stable localized modes [47–50].

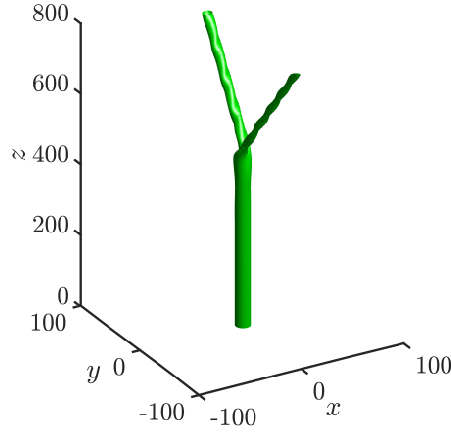


FIG. 9. The evolution of an unstable vortex soliton with $\alpha = 1.5$, $c = 0.2$ and $k = 0.14$, as produced by simulations of Eq. (18) and shown by means of the isosurface of the local intensity $|u(x, y)|^2 = 0.414$. The power of this soliton is $P = 103.01 < P_{\min} \approx 129.17$, see Fig. 6(b). The instability splits the vortex in the set of two localized modes moving in the y direction (perpendicular to the velocity c), which are close to stable fundamental solitons.

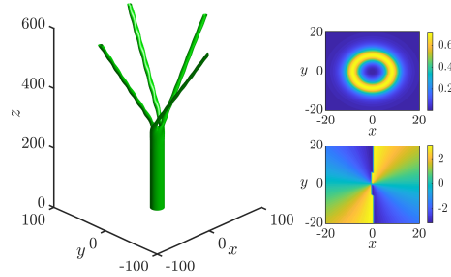


FIG. 10. The same as in Fig. 8, but for an unstable quiescent double-vortex soliton, with $m = 2$, $\alpha = 1.5$, $c = 0$ and $k = 0.1$, as produced by simulations of Eq. (12). The spontaneous splitting of the vortex into the set of separating quasi-solitons is shown by means of the isosurface of the local intensity, $|u(x, y)|^2 = 0.355$. The right top and bottom plots display the initial amplitude and phase profiles of the vortex soliton.

ACKNOWLEDGEMENTS

The Work of T.M. is supported by Faculty of Engineering, Naresuan University through No. The work of B.A.M. is supported, in paper, by Israel Science Foundation through grant No. 1695/22.

[1] N. H. Abel, Oplösning af et Par Opgaver ved Hjelp af bestemte Integraler, Magazin for Naturvidenskaberne. Kristiania (Oslo), pp. 55–68 (1823).
 [2] J. Liouville, Mémoire sur quelques questions de géométrie et de mécanique, et sur un nouveau genre de calcul pour résoudre ces questions, Journal de l'École Polytechnique Paris **13**, 1–69 (1832).
 [3] V. V. Uchaikin, *Fractional Derivatives for Physicists and Engineers* (Springer, New York, 2013).
 [4] M. Caputo, Linear model of dissipation whose Q is almost frequency independent. II, Geophysical Journal International **13**, 529–539 (1967).
 [5] N. Laskin, Fractional quantum mechanics and Lévy path integrals. Phys. Lett. A **268**, 298-305 (2000).
 [6] N. Laskin, *Fractional quantum mechanics* (World Scientific: Singapore, 2018).
 [7] S. Albeverio, R. Hoegh-Krohn, and S. Mazzucchi, *Mathematical Theory of Feynman Path Integrals: An Introduction* (Springer, Berlin and Heidelberg, 2008).
 [8] B. B. Mandelbrot, *The Fractal Geometry of Nature* (W. H. Freeman, New York, 1982).
 [9] X. Guo and M. Xu, Some physical applications of fractional Schrödinger equation, J. Math. Phys. **47**, 082104 (2006).
 [10] M. Cai and C. P. Li, On Riesz derivative, Fractional Calculus and Applied Analysis **22**, 287-301 (2019).
 [11] Pitaevskii L. P. and S. Stringari, *Bose-Einstein Condensation* (Oxford University Press, Oxford, 2003).
 [12] S. Longhi, Fractional Schrödinger equation in optics. Opt. Lett. **40**, 1117-1120 (2015).

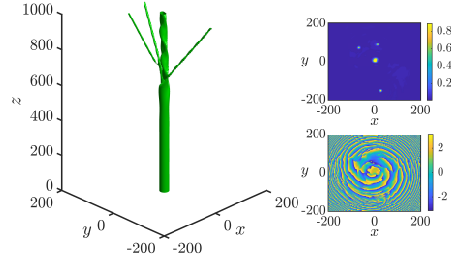


FIG. 11. An example of the splitting instability of a moving vortex soliton with $m = 2$, $c = 0.03$, $k = 0.14$, as produced by simulations of Eq. (12) with $\alpha = 1.5$. The spontaneous separation of low-power jets from the persistent central quasi-solitons is shown by means of the isosurface of the local intensity, $|u(x, y)|^2 = 0.415$. The right top and bottom plots display the final amplitude and phase profiles of the optical field, at $z = 1000$.

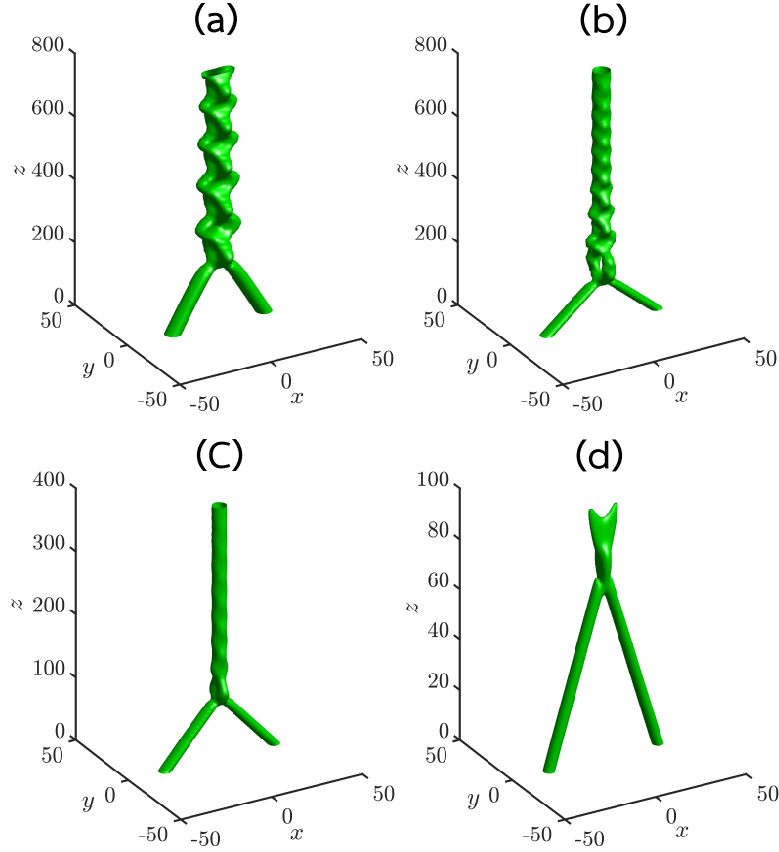


FIG. 12. Outcomes of collisions between moving fundamental solitons with the propagation constant $k = 0.135$ and velocities $c = \pm 0.1$ (a), ± 0.2 (b), ± 0.3 (c), and ± 0.4 (d). The results are produced by simulations of Eq. (12) with $\alpha = 1.5$, and are shown by means of the isosurface of the local intensity (a) $|u(x, y)|^2 = 0.336$; (b) $|u(x, y)|^2 = 0.392$; (c) $|u(x, y)|^2 = 0.370$; (d) $|u(x, y)|^2 = 0.113$; . The outcomes of the collision are merger of the fundamental solitons into robust quiescent breathers in (a) and (b), merger into a stationary quiescent soliton in (c), and destruction of the colliding solitons in (d). The latter outcome is observed in interval (20) of the collision velocities.

- [13] Y. S. Kivshar and G. P. Agrawal, *Optical Solitons: From Fibers to Photonic Crystals* (Academic Press, San Diego, 2003).
- [14] S. Liu, Y. Zhang, B. A. Malomed, and E. Karimi, Experimental realisations of the fractional Schrödinger equation in the temporal domain, *Nature Comm.* **14**, 222 (2023).
- [15] C. Klein, C. Sparber, and P. Markowich, Numerical study of fractional nonlinear Schrödinger equations. *Proc. R. Soc. A* **470**, 20140364 (2014).
- [16] S. Duo and Y. Zhang, Mass-conservative Fourier spectral methods for solving the fractional nonlinear Schrödinger equation, *Computers and Mathematics with Applications* **71**, 2257-2271 (2016).

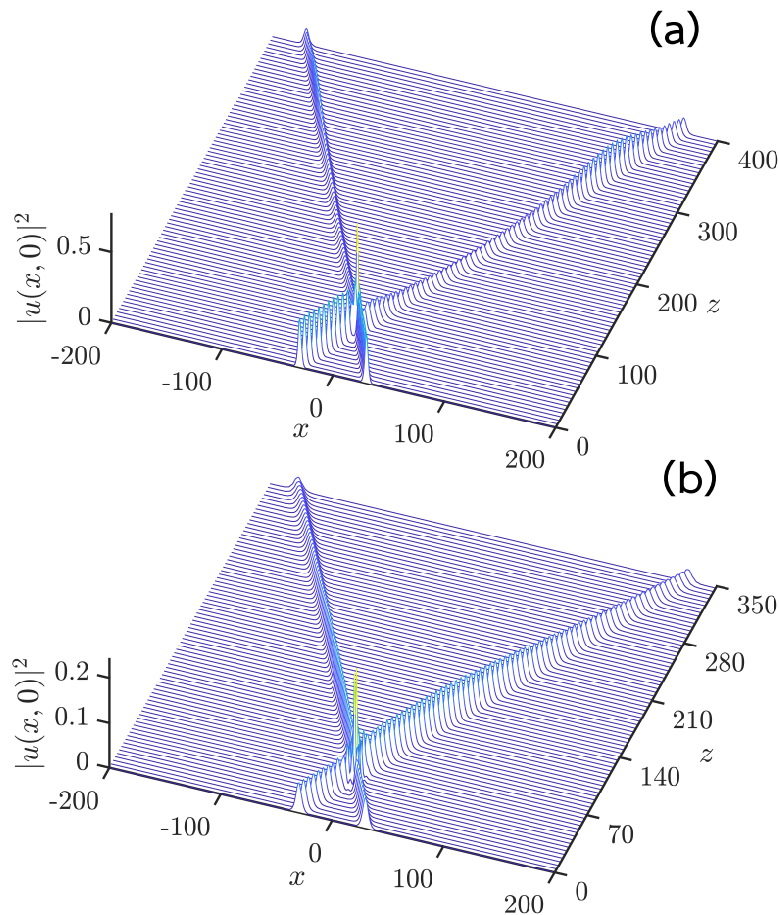


FIG. 13. Quasi-elastic collisions between the moving fundamental solitons with $\alpha = 1.5$ and $k = 0.135$, shown by means of the evolution of the local power (intensity) in cross section $y = 0$ for collision velocities $c = \pm 0.50$ (a) and $c = \pm 0.59$ (b).

- [17] S. Secchi and M. Squassina, Soliton dynamics for fractional Schrödinger equations, *Applicable Analysis*, **93**, 1702-1729 (2014).
- [18] C. M. Huang and L. W. Dong, Gap solitons in the nonlinear fractional Schrodinger equation with an optical lattice, *Opt. Lett.* **41**, 5636-5639 (2016).
- [19] M. Chen, S. Zeng, D. Lu, W. Hu, and Q. Guo, Optical solitons, self-focusing, and wave collapse in a space-fractional Schrödinger equation with a Kerr-type nonlinearity, *Phys. Rev. E* **98**, 022211 (2018).
- [20] L. W. Dong, C. M. Huang, and W. Qi, Nonlocal solitons in fractional dimensions, *Opt. Lett.* **44**, 4917-4920 (2019).
- [21] B. A. Malomed, Optical solitons and vortices in fractional media: A mini-review of recent results, *Photonics* **8**, 353 (2021).
- [22] L. Bergé, Wave collapse in physics: principles and applications to light and plasma waves, *Phys. Rep.* **303**, 259-370 (1998).
- [23] G. Fibich, *The Nonlinear Schrödinger Equation: Singular Solutions and Optical Collapse* (Springer, Heidelberg, 2015).
- [24] R. Y. Chiao, E. Garmire, and C. H. Townes, Self-trapping of optical beams, *Phys. Rev. Lett.* **13**, 479-482 (1964).
- [25] G. Boudebs, S. Cherukulappurath, H. Leblond, J. Troles, F. Smektala, and F. Sanchez, Experimental and theoretical study of higher-order nonlinearities in chalcogenide glasses, *Opt. Commun.* **219**, 427-432 (2003).
- [26] L. Falcão Filho, C. B. de Araújo, G. Boudebs, H. Leblond, and V. Skarka, Robust two-dimensional spatial solitons in liquid carbon disulfide, *Phys. Rev. Lett.* **110**, 013901 (2013).
- [27] A. S. Reyna. and C. B. de Araújo, High-order optical nonlinearities in plasmonic nanocomposites – a review, *Adv. Opt. Phot.* **9**, 720-774 (2017).
- [28] O. Reshef, E. Giese, M. Z. Alam, I. de Leon, J. Upham, and R. W. Boyd, Beyond the perturbative description of the nonlinear optical response of low-index materials, *Opt. Lett.* **42**, 3225-3228 (2017).
- [29] M. Quiroga-Teixeiro and H. Michinel, Stable azimuthal stationary state in quintic nonlinear optical media, *J. Opt. Soc. Am. B* **14**, 2004-2009 (1997).
- [30] R. L. Pego and H. A. Warchall, Spectrally stable encapsulated vortices for nonlinear Schrödinger equations, *J. Nonlinear Sci.* **12**, 347-394 (2002).
- [31] L. W. Zeng and J. H. Zeng, One-dimensional gap solitons in quintic and cubic-quintic fractional nonlinear Schrödinger equations with a periodically modulated linear potential, *Nonlin. Dynamics* **98**, 985-995 (2019).

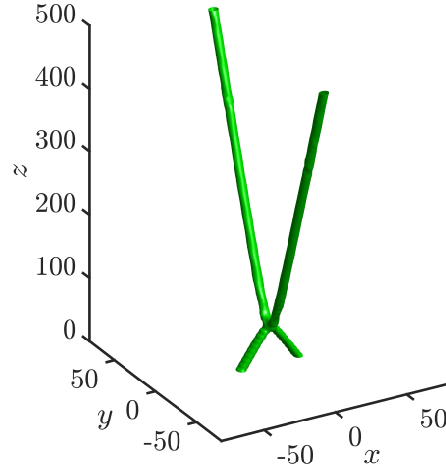


FIG. 14. The quasi-elastic collision between fundamental solitons with $c = \pm 0.3$ for $\alpha = 1.0$ and $k = 0.09$, shown by means of the isosurface of the local intensity, $|u(x, y)|^2 = 0.3419$. After the collision, the solitons move in the perpendicular direction. The collisions follow this scenario in interval (21).

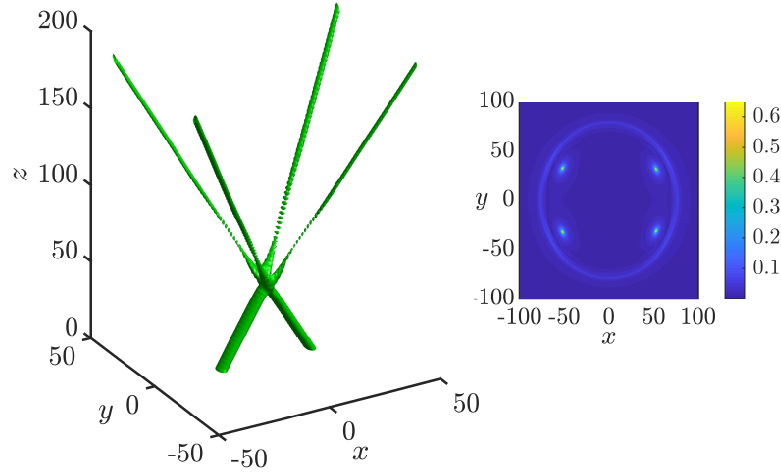


FIG. 15. (Left) The inelastic collision between the fundamental solitons with $\alpha = 1.0$, $k = 0.09$, and velocities $c = \pm 0.4$, shown by means of the isosurface of the local intensity, with $|u(x, y)|^2 = 0.216$. (Right) The intensity profile at $z = 200$, which shows the set of four secondary solitons produced by the collision. This outcome of the collisions occurs in the interval of velocities $0.36 < |c| < c_{\max} \approx 0.49$.

- [32] P. Li and C. Dai, Double loops and pitchfork symmetry breaking bifurcations of optical solitons in nonlinear fractional Schrödinger equation with competing cubic-quintic nonlinearities, *Ann. Physik (Berlin)* **532**, 2000048 (2020).
- [33] Y. Qiu, B. A. Malomed, D. Mihalache, X. Zhu, X. Peng, and Y. He, Stabilization of single- and multi-peak solitons in the fractional nonlinear Schrödinger equation with a trapping potential, *Chaos, Solitons & Fractals* **140**, 110222 (2020).
- [34] L. Zeng, D. Mihalache, B. A. Malomed, X. Lu, Y. Cai, Q. Zhu, and J. Li, Families of fundamental and multipole solitons in a cubic-quintic nonlinear lattice in fractional dimension, *Chaos, Solitons & Fractals* **144**, 110589 (2021).
- [35] K. Manikandan, D. Aravintan, and J. B. Sudharsan, and R. Vadivel, Optical solitons in the generalized space-time fractional cubic-quintic nonlinear Schrödinger equation with a \mathcal{PT} -symmetric potential, *Optik* **271**, 170105 (2022).
- [36] Y. X. Chen, and X. Xiao, Combined soliton solutions of a (1+1)-dimensional weakly nonlocal conformable fractional nonlinear Schrödinger equation in the cubic-quintic nonlinear material, *Opt. Quant. Electr.* **53**, 21 (2021).
- [37] V. A. Stephanovich, W. Olchawa, E. V. Kirichenko, and V. K. Dugaev, 1D solitons in cubic-quintic fractional nonlinear Schrödinger model, *Scient. Rep.* **12**, 15031 (2022).
- [38] A. Houwe, S. Abbagari, P. Djourwe, Y. Saliou, S. Y. Doka, and M. Inc, W-shaped profile and breather-like soliton of the fractional nonlinear Schrödinger equation describing the polarization mode in optical fibers, *Opt. Quant. Electr.* **54**, 483 (2022).
- [39] W. J. Chen, C. Lian, and Y. A. Luo, Interaction of Airy beams modeled by the fractional nonlinear cubic-quintic Schrödinger equation, *Physica Scripta* **96**, 125256 (2021).

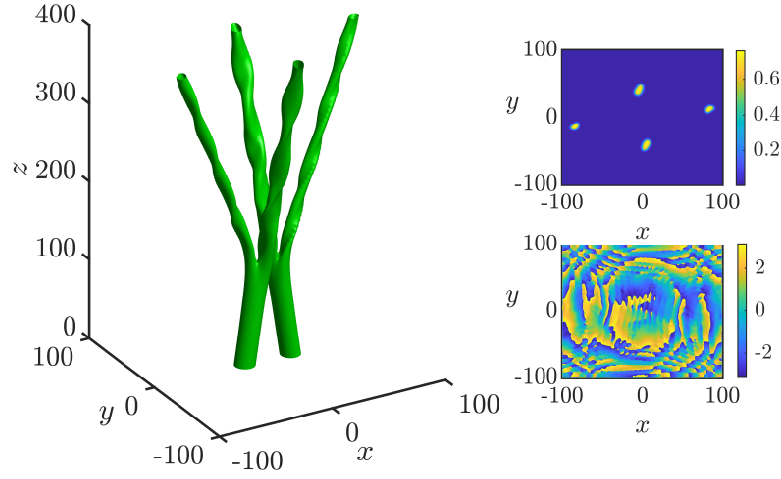


FIG. 16. (Left) The collision between two identical vortex solitons with winding numbers $m = 1$, propagation constant $k = 0.14$ and velocities $c = \pm 0.1$, produced by simulations of Eq. (12) with $\alpha = 1.5$. The result is shown by means of the isosurface of the local intensity $|u(x, y)|^2 = 0.380$. (Right) The intensity and phase profiles at $z = 400$, which show the set of four secondary quasi-solitons produced by the collision. The emerging elliptically deformed quasi-solitons rotate counter-clockwise, keeping the original angular momentum of the colliding vortices. This example illustrates the outcome of the collision between counterpropagating identical vortex solitons observed in the generic case.

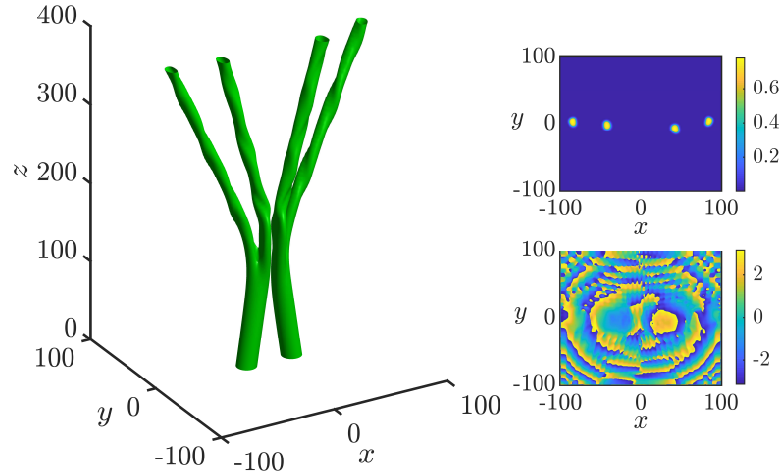


FIG. 17. The same as in Fig. 16, but for the collision of the vortex solitons with winding numbers $m = +1$ and -1 .

- [40] J. G. Zhang, Modulation instability in fractional Schrödinger equation with cubic-quintic nonlinearity, *J. Nonlin. Opt. Phys. & Materials* **31**, 2250019 (2022).
- [41] L. W. Zeng and J. H. Zeng, Preventing critical collapse of higher-order solitons by tailoring unconventional optical diffraction and nonlinearities, *Communications Physics* **3**, 26 (2020).
- [42] M. Zhong, Two-dimensional fractional PPT-symmetric cubic-quintic NLS equation: Double-loop symmetry breaking bifurcations, ghost states and dynamics, *Physica D* **448**, 133727 (2023).
- [43] P. Li, B. A. Malomed, and D. Mihalache, Vortex solitons in fractional nonlinear Schrödinger equation with the cubic-quintic nonlinearity, *Chaos, Solitons & Fractals* **137**, 109783 (2020).
- [44] P. Li, B. A. Malomed, and D. Mihalache, Metastable soliton necklaces supported by fractional diffraction and competing nonlinearities, *Opt. Exp.* **28**, 34472-34488 (2020).
- [45] N. G. Vakhitov N. G. and A. A. Kolokolov, Stationary solutions of the wave equation in a medium with nonlinearity saturation, *Radiophys. Quantum Electron.* **16**, 783-789 (1973); <https://doi.org/10.1007/BF01031343>.
- [46] J. Yang and T. Lakoba, Universally-convergent squared-operator iteration methods for solitary waves in general nonlinear wave equations, *Stud. Appl. Math.* **118**, 153-197 (2007).
- [47] S. Sirisubtawee, S. Koonprasert, S. Sungnul, and T. Leekparn, Exact traveling wave solutions of the space-time fractional complex Ginzburg-Landau equation and the space-time fractional Phi-4 equation using reliable methods, *Advances in Differential Equation*, article No. 219 (2019).

- [48] Y. Qiu, B. A. Malomed, D. Mihalache, X. Zhu, L. Zhang, and Y. He, Soliton dynamics in a fractional complex Ginzburg-Landau model, *Chaos, Solitons and Fractals* **131**, 109471 (2020).
- [49] J. X. Yang, X. Zhu, X. Peng, Y. J. He, X. J. Wang, and Y. L. Qiu, Elliptic vortex beam in a fractional complex Ginzburg-Landau model, *J. Optics* **23**, 15503 (2021).
- [50] D.-S. Mou, J.-J. Fang, and Y. Fan, Discrete localized excitations for discrete conformable fractional cubic–quintic Ginzburg-Landau model possessing the non-local quintic term, *Optik* **244**, 167554 (2021).